Quantification of surface water volume changes in the Mackenzie Delta using satellite multi-mission data

Cassandra Normandin[1], Frédéric Frappart[2, 3], Bertrand Lubac[1], Simon Bélanger[4], Vincent Marieu[1], Fabien Blarel[3], Arthur Robinet[1] and Léa Guiastrennec-Faugas[1]

[1] EPOC, UMR 5805, Université de Bordeaux, Allée Geoffroy Saint-Hilaire, 33615 Pessac, France
[2] GET-GRGS, UMR 5563, CNRS/IRD/UPS, Observatoire Midi-Pyrénées, 31400 Toulouse, France
[3] LEGOS-GRGS, UMR 5566, CNRS/IRD/UPS, Observatoire Midi-Pyrénées, 31400 Toulouse, France
[4] Dép. Biologie, Chimie et Géographie, groupe BOREAS and Québec-Océan, Université du Québec à Rimouski, 300 allée des ursulines, Rimouski, Qc, G5L 3A1, Canada

Correspondence to: Cassandra Normandin (cassandra.normandin@u-bordeaux.fr)

Abstract. Quantification of surface water storage in extensive floodplains and their dynamics are crucial for a better understanding of global hydrological and biogeochemical cycles. In this study, we present estimates of both surface water extent and storage combining multi-missions remotely-sensed observations and their temporal evolution over more than 15 years in the Mackenzie Delta. The Mackenzie Delta is located in the North West of Canada and is the second largest delta in the Arctic Ocean. The delta is frozen from October to May and the recurrent ice break up provokes an increase of the river's flows. Thus, this phenomenon causes intensive floods along the delta every year with dramatic environmental impacts. In this study, the dynamics of surface water extent and volume are analyzed from 2000 to 2015 by combining multi-satellite information from MODIS multispectral images at 500 m spatial resolution and river stages derived from ERS-2 (1995-2003), ENVISAT (2002-2010) and SARAL (since 2013) altimetry data. The surface water extent (permanent water and flooded area) peaked in June with an area of 9,600 km² (+/- 200 km²) on average, representing approximately 70% of the delta's total surface. Altimetry-based water levels exhibit annual amplitudes ranging from 4 m in the downstream part to more than 10 m in the upstream part of the Mackenzie Delta. A high overall correlation between the satellite-derived and in situ water heights (R>0.84) is found for the three altimetry missions. Finally, using altimetry-based water levels and MODIS-derived surface water extents, maps of interpolated water heights over the surface water extents are produced. Results indicate a high variability of the water height magnitude that can reach 10 meters compared to the lowest water height in the upstream part of the delta during the flood peak in June. Furthermore, the total surface water volume is estimated and shows an annual variation of approximately 8.5 km^3 during the whole study period, with a maximum of 14.4 km^3 observed in 2006. The good agreement between the total surface water volume retrievals and in situ river discharges (R=0.66) allows validating this innovative multi-mission approach and highlights the high potential to study the surface water extent dynamics.

Key words: Mackenzie Delta, surface water extent, multispectral imagery, satellite altimetry, surface water volume

1 Introduction

Deltas are vulnerable to both anthropogenic and natural forcing such as socio-economic infrastructure development and global warming. In Arctic, the latter is particularly severe due to the polar amplification processes and complex positive feedback loops (Holmes et al., 2012). This system is undergoing important changes as the increase of precipitation at high latitudes, increase river discharge and melting of stock ices on land and sea (Stocker and Raible, 2005). These changes may induce an acceleration of the hydrologic cycle (Stocker and Raible, 2005). River discharge may increase from 18 to 70% from now to the end of the century (Peterson et al., 2002). Improving our knowledge on the dynamics of the surface water reservoir in circumpolar areas is crucial for a better understanding of their role in flood hazard, carbon production, greenhouse gases emission, sediment transport, exchange of nutrients and land-atmosphere interactions.

Mapping surface water extent at the Mackenzie Delta scale is an important issue. However, it is nearly impossible to provide a long-term monitoring with traditional methods using in-situ measurements in such a large and heterogeneous environment. Satellite remote sensing methods offers a unique opportunity for the continuous observation of wetlands and floodplains. Remote sensing has proven a strong potential to detect and monitor floods during the last two decades (Alsdorf et al., 2007; Smith, 1997). Typically, two kinds of sensor are used to map flooded area at high and moderate resolutions: passive multispectral imagery and active Synthetic Aperture Radar (SAR). The spectral signature of the surface reflectance is used to discriminate between water and land (Rees, 2013). The SAR images provide valuable information on the nature of the observed surface through the backscattering coefficient (Ulaby et al., 1981).

If space missions of radar altimetry were mainly dedicated to estimate ocean surface topography (Fu and Cazenave, 2001), it is now commonly used for monitoring inland waters levels (Birkett, 1995 ; Cazenave et al., 1997; Frappart et al., 2006a; Santos da Silva et al., 2010; Crétaux et al., n.d.; Frappart et al., 2015b; Crétaux et al., 2017). Several studies have shown the possibility to measure water levels variations in lakes, rivers and flooding plains (Frappart et al., 2006b, 2015a; Santos da Silva et al., 2010). In the present study, satellite multispectral imagery and altimetry are used in synergy to quantify surface water extents and the surface water volumes of the Mackenzie Delta and analyze their temporal variations. In the past, this approach has been applied in tropical (e.g., the Amazon (Frappart et al., 2012), Mekong (Frappart et al., 2006b)) and peri-Arctic (e.g. the Lower Ob' basin, (Frappart et al., 2010) major river basins allowing to provide direct observations of the spatio-temporal dynamics of surface water storage. Several limitations prevent them to be used over estuaries and deltas. The first is the too coarse spatial resolution of the datasets used for retrieving the flood extent that ranges from 1 km with SPOT-VGT images used in the Lower Mekong Basin to ~ 0.25° with the Global Inundation Extent from Multi-Satellite (GIEMS, Papa et al., 2010) for the Lower Ob' and the Amazon basins. The second is inherent to the datasets used in these studies. For the Mekong Basin, due to the limited number of spectral bands present in the VGT sensor, a mere threshold on NDVI was applied. For the Amazon and the Lower Ob', as GIEMS dataset is using surface temperatures from SSM/I, no valid data are available at less than 50 km from the coast. The originality and novelty of the study is the use of multi-space mission data at better spatial, temporal and spectral resolutions than the previous studies to monitor surface water storage changes in a deltaic environment over a fifteen-year time period.

Earlier studies pointed out i) the lack of continuous information in the Mackenzie delta to study the spatial distribution of water levels during the flood events and to analyze the relationship between flood severity and the

timing and duration of break-up in the delta (Goulding et al, 2009b; Beltaos et al., 2012), ii) the importance of the tributaries to the Mackenzie River (i.e., Peel and Arctic Red rivers) on break-up and ice-jam flooding in the delta (Goulding et al., 2009a). As the goal of this study is to characterize the spatio-temporal dynamics of surface water, both in surface and storage, in the Mackenzie delta, north west territories of Canada, in response to spring ice break-up and snow melt, over the period 2000-2015, it will provide important new information for a better understanding of the hydro-climatology of the region.

2 Study region

The Mackenzie Delta, a floodplain system, is located in the northern part of Canada (Figure 1a) and covers an area of 13,135 km² (Emmerton et al., 2008), making it the second biggest delta of Arctic with a length of 200 km and a width of 80 km (Emmerton et al., 2008). It is mainly drained by the Mackenzie River (90% of the delta's water supply) and Peel River (8% of the delta's water supply, Emmerton et al., 2007). The Mackenzie Delta channels have very mild slopes (-0.02 m/km, (Hill et al., 2001) and is ice covered during 7-8 months per year (Emmerton et al., 2007).

The Mackenzie River begins in the Great Slave Lake and then, flows through the North West territories before reaching the Beaufort Sea. It has a strong seasonality in term of discharge due to spring ice break-up and snowmelt, from about 5,000 $m^3.s^{-1}$ in winter up to 40,000 $m^3.s^{-1}$ in June during the ice breakup for wet years (Figure 1b, Macdonald and Yu, 2006 ; Goulding et al., 2009a ; Goulding et al., 2009b ; Beltaos et al., 2012). The Stamukhi (ground accumulation of sea ice) is responsible for recurrent floods in the Mackenzie Delta. At the flood peak, 95% of the delta surface is likely to be covered with water (Macdonald and Yu, 2006). Water level peaks are mainly controlled by ice breakup effects and secondary by the amount of water contained in snowpack (Lesack and Marsh, 2010). This is one of the most important annual hydrologic events in cold regions (Muhammad et al., 2016).

The delta is a complex of multiple channels and numerous shallow and small lakes (over 49,000 lakes), covering nearly ~50% of the delta area (Emmerton et al., 2007), and are ecologically sensitive environments largely controlled by river water (Squires et al., 2009). This environment is also one of the most productive ecosystems in northern Canada with large populations of birds, fishes and mammals, which are critical resources for local population (Squires et al., 2009).

3 Data sets

3.1 Multispectral imagery

3.1.1 MODIS

The MODerate resolution Imaging Sensor (MODIS) is a spectroradiometer, part of the payload of the Aqua (since 2002) and Terra (since 1999) satellites. The MODIS sensor measures radiances in 36 spectral bands. In this study, the MOD09A1 product (8-day binned level 3, version 6) derived from Terra satellite surface reflectance measurements were downloaded from the United States Geological Survey (USGS) Earthexplorer website (http://earthexplorer.usgs.gov). It consists in gridded, atmospherically corrected surface reflectance acquired in 7 bands from visible to short wave infrared (2155 nm) at a 500 m spatial resolution. This product is obtained combining for each wavelength the best surface reflectance data of every pixel acquired during an 8-day period.

Each MODIS tile covers an area of 1200 km by 1200 km. Two tiles (h12v02 and h13v02) are used to cover the whole study area. In this study, 223 composites, acquired during the ice-free period from June to September over the 2000-2015 time-span, are used.

3.1.2 OLI

The Landsat-8 satellite is composed of two Earth-observing sensors, the Operational Land Imager (OLI) and Thermal InfraRed Sensor (TIRS). This satellite was launched in February 2013 and orbits at an altitude of 705 km. The swath is 185 km and the whole Earth surface is covered every 16 days.

The OLI/TIRS sensors measure in 11 spectral bands in the visible (450-680 nm), near infrared (845-885 nm) and short wave infrared portions (1,560-2,300 nm) of the electromagnetic spectrum. In this study, the Landsat 8/OLI surface reflectance products were downloaded from the Landsat-8 USGS portal (http://earthexplorer.usgs.gov/). The multispectral spatial resolution is 30 m and 15 m for panchromatic band. Two images are necessary to cover the Mackenzie Delta.

Landsat-8 mission is characterized by a lower revisit time than Terra and Aqua mission. Thus, associated with a high occurrence of clouds over the study area, Landsat-8 yields to a small amount of high-quality data. OLI images cannot be consequently used in this study to monitor land water surface temporal changes. In this context, MODIS represent a relevant alternative to OLI despite a lower spatial resolution. However, available high-quality OLI data have been used to compare and validate MODIS land water surfaces.

3.2 Radar altimetry data

3.2.1 ERS-2

The ERS-2 satellite (European Remote Sensing) was launched in 1995 by the European Space Agency (ESA). Its payload is composed of several sensors, including a radar altimeter (RA), operating at Ku-band (13.8 GHz). It was orbiting sun-synchronously at an altitude of 790 km with an inclination of 98.54° with a 35-day repeat cycle. This orbit was ERS-1's orbit with a ground-track spacing about 85 km at the equator. ERS-2 provides observations of the topography of the Earth from 82.4° latitude north to 82.4° latitude south. ERS-2 data are disposable from 17 May 1995 to 9 August 2010 but after 22 June 2003, the coverage is limited.

3.2.2 ENVISAT

Envisat mission was launched on March 1st 2002 by ESA. This satellite carried 10 different instruments including the advanced radar altimeter (RA-2). It was based on the heritage of ERS-1 and 2 satellites. RA-2 was a nadir-looking pulse-limited radar altimeter operating at two frequencies at Ku- (13.575 GHz) and S-(3.2 GHz) bands. Its goal was to collect radar altimetry over ocean, land and ice caps (Zelli, 1999). Envisat remained on its nominal orbit until October 2010 but RA-2 stopped operating correctly at S-band in January 2008. Its initial orbital characteristics are the same as for ERS-2.

3.2.3 SARAL

SARAL mission was launched on 25 February 2013 by a partnership between CNES (Centre National d'Etudes Spatiales) and ISRO (Indian Space Research Organization). Its payload comprised the AltiKa radar altimeter and

bi-frequency radiometer, and a triple system for precise orbit determination: the real-time tracking system DIODE of DORIS instrument, a Laser Retroflector Array (LRA), and the Advance Research and Global Observation Satellite (ARGOS-3). AltiKa is the first radar altimeter to operate Ka-band (35.75 GHz). It is a solid-state mono-frequency altimeter that provides precise range estimates (Verron et al., 2015). SARAL orbit was earlier utilized by ERS-1 & 2 and ENVSAT missions with a track spacing of 85 km at the equator (Verron et al., 2015). It has been put on a drifting orbit since 4 July 2016.

Altimetry data used here are contained in the Geophysical Data Records (GDRs) and are the followings:

- cycle 001 (17/05/1995) to cycle 085 (07/08/2003) for ERS-2 from the reprocessing of the ERS-2 mission raw waveform performed at Centre de Topographie de l'Océan et de l'Hydrosphère (CTOH) (Frappart et al., 2016)
- GDR v2.1 for ENVISAT from cycle 006 (14/05/2002) to cycle 094 (21/10/2010)
- GDR E for SARAL from cycle 001 (15/03/2015) to cycle 027 (14/10/2015)

These data were made available by CTOH (http://ctoh.legos.obs-mip.fr/). Data were acquired along the altimeter track at 18, 20 and 40 Hz for ENVISAT, ERS -2 and SARAL respectively (high-frequency mode commonly used over land and coastal areas where the surface properties are changing more rapidly than over the open ocean). They consist of the satellite locations and acquisition times and all the parameters necessary to compute the altimeter heights (see Section 4.3).

3.3 In situ water levels and discharges

The altimetry-based water level time-series derived from radar altimetry were compared to gauge record from in situ stations for validation purpose. Data from 10 gauge stations were found in a close vicinity of altimetry virtual stations (at a distance lower than 20 km along the streams). Virtual stations are built at intersections between an orbit groundrack and a water body (lake, river and floodplain) (Crétaux et al., 2017). Besides, surface water storage variations were compared to the rivers flow entering the delta summing the records from 3 gauge stations located in upstream part of the delta. Daily data of water level and discharge were downloaded for free from the Canadian government website (http://wateroffice.ec.gc.ca).

4 Methods

4.1 Quantification of surface water extent

Multispectral imagery is commonly used for delineating flood extent using spectral indices (e.g., Frappart et al., 2006b; Sakamoto et al., 2007; Crétaux et al., 2011; Verpoorter et al., 2014; Ogilvie et al., 2015; Pekel et al., 2016). As we do not have any external information to perform a supervised classification as the current state of the art machine learning techniques (Pekel et al., 2016; Tulbure et al., 2016; Klein et al., 2017), we used the approach proposed by (Sakamoto et al., 2007) to monitor the land water surface extent in the Mackenzie Delta (Figure 2). This approach is based on the application of thresholds on the Enhanced Vegetation Index (EVI), the Land Surface Water Index (LSWI) and the Difference Value between EVI and LSWI (DVEL=EVI-LSWI) to determine the status (non-flooded, mixed, flooded and permanent water body) of any pixel in an 8-day MODIS composite image of surface reflectance. As the spectral response of the Near Infra-Red (NIR) and short-wave infrared (SWIR) bands are highly dependent on the Earth surface nature, in particular water versus soil/vegetation surfaces, their

complementary was used to define LSWI. For instance, the surface reflectance presents low values (a few percentages) over non-turbid water bodies and high values (a few tens of percentage) over vegetation feature in the NIR spectral bands. The spectral response in the SWIR is mainly dominated by strong water absorption bands, which is directly sensitive to moisture content in the soil and the vegetation. For water surface, the signal in the SWIR is assumed to be zero even in turbid waters (Wang and Shi, 2005). Thus, LSWI is expected to get values close to 1 for water surfaces and lower values for non-water surfaces.

The two indices, used in this approach, are defined as follows (Huete et al., 1997; Xiao et al., 2005):

$$EVI = a \times \frac{\rho_{NIR} - \rho_{red}}{\rho_{NIR} + b \times \rho_{red} - c \times \rho_{blue} + d} \quad (1)$$

$$LSWI = \frac{\rho_{NIR} - \rho_{SWIR}}{\rho_{NIR} + \rho_{SWIR}} \quad (2)$$

where for MODIS, ρ_{blue} is the surface reflectance value in the blue (459-479 nm, band 3), ρ_{red} is the surface reflectance value in the red (621-670 nm, band 1), ρ_{NIR} is the surface reflectance value in the NIR (841-875 nm, band 2), and ρ_{SWIR} is the surface reflectance in the SWIR (1628-1652 nm, band 6). For OLI, ρ_{blue}, ρ_{red}, ρ_{NIR} and ρ_{SWIR} are associated to channel 2 (452-512 nm), channel 4 (636-673 nm), channel 5 (851-879 nm), and channel 6 (1570-1650 nm). *a*, *b*, *c* and *d* constants equal to 2.5, 6, 7.5 and 1, respectively, for both MODIS and OLI (USGS, product guide).

To process multispectral images, the first step consists in removing the cloud-contaminated pixels applying a cloud masking based on a threshold of the surface reflectance in the blue band ($\rho_{blue} \geq 0.2$). Then, spectral indices are computed. Note that, contrary to (Sakamoto et al., 2007), no smoothing was applied on spectral indices time-series. In a second step, the identification of the status of each pixel is performed applying thresholds on EVI, LSWI and their differences (Figure 2), which reduce the noise component. Thresholds determined by Sakamoto et al. (2007) were validated for our study site using OLI images acquired on 01/07/2013 and 02/08/2013 and compared to MODIS (Figure S1). Histograms show a similar bi-modal distribution for both EVI, LSWI and EVI-LSWI between MODIS and OLI 500 m (Figure S1 andS2). For EVI, pixels with a value lower than 0.1 are clearly associated with water land surfaces, while pixels with a value higher than 0.3 are associated with soil and vegetation features. Other pixels, with an EVI value comprised between 0.1 and 0.3, are identified as mixed surface types. For LSWI, pixels with a value higher than 0.5 are clearly associated with water land surfaces, while pixels with a value lower than 0.3 are associated with vegetation features or soil land surfaces when LSWI values are negative. Other pixels, with an LSWI value comprised between 0.3 and 0.5, are identified as mixed surface types. Contrary to what was found by Sakamoto et al. (2007) in the Mekong Basin, no negative value of LSWI were observed over our study area. This threshold was not applied in this study. For EVI-LSWI, pixels with a value lower than -0.05 are represented water land surface and values comprised between -0.05 and 0.1 are associated to mixed pixels. Other pixels, with values higher than 0.1 are represented vegetation features or soil land surfaces (Figure S2). Each pixel was then classified in two main categories: non-flooded (EVI > 0.3 or EVI ≤ 0.3 but EVI – LSWI > 0.05) and water-influenced (EVI ≤ 0.3 and EVI – LSWI ≤ 0.05 or EVI ≤ 0.05) (Figure 2). The second category was divided into three sub-classes: mixed pixels (0.1< EVI ≤ 0.3), flooded pixels (EVI ≤ 0.1) and permanent water bodies (e.g. lake, river and sea), when the total duration of a pixel classified as flooded is longer than 70 days out of 105 day for the study period. This annual duration for our study corresponds roughly to 2/3 of the study period, as proposed by Sakamoto et al. (2007). The spatio-temporal variations of floods have been characterized for the months included between June and September over the 2000-2015 period.

Thereafter, we define in this paper land water surface as permanent water bodies with flooded areas although inundated surfaces including only inundated areas.

4.2 Validation of MODIS retrievals using OLI

Evaluation of the performance of the land water surface detection from MODIS is based on the comparison between land surface water estimated from MODIS at a 500 m-resolution, OLI at a 30 m-resolution, and OLI re-sampled at 500 m-resolution. For the validation purpose, MODIS and OLI images are selected when (1) the time-difference between the acquisitions of two satellite images is lower than 3 days and (2) the presence of cloud over the area is lower than 5%. Following these criteria, only two cloud-free OLI composites were selected between 1st July 2013 and 2nd August 2013.

4.3 Satellite-derived water level time-series in the Mackenzie Delta

The concept of radar altimetry is explained below. The radar emits an electromagnetic (EM) wave towards the surface and measures the round-trip time (Δt) of the EM wave. Taking into account propagation corrections caused by delays due to the interactions of electromagnetic wave in the atmosphere, and geophysical corrections, the height of the reflecting surface (h) with reference to an ellipsoid can be estimated as (Crétaux et al., 2017):

$$h = H - (R + \sum \Delta R_{propagation} + \Delta R_{geophysical}) \quad (3)$$

where H is the satellite center of mass height above the ellipsoid, R is the nadir altimeter range from the satellite center of mass to the the surface taking into account instrument corrections ($R = c\Delta t/2$ where c is the light velocity in the vacuum), $\sum \Delta R_{propagation}$ is the sum of the geophysical and environmental corrections applied to the range, respectively.

$$\sum \Delta R_{propagation} = \Delta R_{ion} + \Delta R_{dry} + \Delta R_{wet} \quad (4)$$

where ΔR_{ion} is the atmospheric refraction range delay due to the free electron content associated with the dielectric properties of the ionosphere, ΔR_{dry} is the atmospheric refraction range delay due to the dry gas component of the troposphere, ΔR_{wet} is the atmospheric refraction range delay due to the water vapor and the cloud liquid water content of the troposphere.

$$\sum \Delta R_{geophysical} = \Delta R_{solid\ Earth} + \Delta R_{pole} \quad (5)$$

where $\Delta R_{solid\ Earth}$ and ΔR_{pole} are the corrections respectively accounting for crustal vertical motions due to the solid Earth and pole tides. The propagation corrections applied to the range are derived from model outputs: the Global Ionospheric Maps (GIM) and Era Interim from the European Centre Medium-Range Weather Forecasts (ECMWF) for the ionosphere and the dry and wet troposphere range delays respectively. The changes of the altimeter height h over the hydrological cycles are related to variations in water level. Here, the Multi-mission altimetry Processing Software (MAPS) was used to precisely select valid altimetry data at every virtual station locations (see part 3.3) series in the Mackenzie Delta. Data processing consists in four steps (Frappart et al., 2015b):

- The rough delineation of the river/lake cross-sections with overlaying altimeter tracks using Google Earth. Distances of plus or minus 5 km from the river banks are generally considered.
- The loading of the altimetry over the study area and the computation of the altimeter heights from the raw data contained in the GDRs,

- Valid altimetry data were selected through a refined process that consists in eliminating outliers and measurements over non-water surfaces based on visual inspection. The shape of the altimeter along-track profiles permit to identify the river that is generally materialized as a shape of "V" or "U" with the lower elevations corresponding to the water surface (see Santos da Silva et al., 2010 and Baup et al., 2014 for more details).
- The computation of the time-series of water level.

4.4 Surface water volume storage

The approach used to estimate the anomalies of surface water volume is based on the combination of the surface water extent derived from MODIS images with altimetry-based water levels estimated at virtual stations distributed all over the delta (Figure 5). Surface water level maps were computed from the interpolation of water levels over the land water surfaces using an inverse-distance weighting spatial interpolation technique following (Frappart et al., 2012). Hence, water level maps were produced every 8 days from 2000 to 2015. For each water pixel, the minimal height of water during 2000-2015 is estimated. As ERS-2, ENVISAT and SARAL had a repeat cycle of 35 days, water levels are linearly interpolated every 8 days to be combined with the MODIS composite images. Surface water volume time series are estimated over the Mackenzie Delta following (Frappart et al., 2012):

$$V=\sum_{j \epsilon S}[h(\lambda_j, \varphi_j) - h_{min}(\lambda_j, \varphi_j)].\delta_j . \Delta S \quad (6)$$

where V is the anomaly of surface water volume (km3), S is the surface of the Mackenzie Delta (km²), h (λj, φj) the water level, $h_{min}(\lambda_j, \varphi_j)$ the minimal water level for the pixel of coordinates (λ_j, φ_j) inside the Mackenzie Delta, δ_j equals 1 if the j^{th} pixel is associated to permanent water body/inundated and 0 if not and ΔS the pixel surface (0.25 km²).

5. Results

5.1 MODIS-based land water extent and their validation

Following Sakamoto et al. (2007) method, all pixels of 8-day image have been classified into 4 classes: class 0 corresponding to vegetation, class 1 to permanent water, class 2 to inundation and class 3 to mixture of land and water. Map of annual average of land water surface, composed of inundated and permanent water bodies (classes 1 and 2), was obtained at spatial and temporal resolutions of 500 m and 8 days respectively from June to September over the 2000-2015 period (Figure 3a). Map of annual average of land water surface duration along with associated standard deviation over 2000-2015 during ice-free period of three months and half (105 days) is presented in Figure 3b. Permanent water bodies (i.e., identified as land water surface more than 70 days annually) are located along the Mackenzie River main channel, its tributaries (Reindeer, Peel, Middle and East Channels) and major lakes of the Delta. The longer water areas (i.e., identified as flooded between 30 and 70 days annually) are surrounding permanent water bodies. Other areas of the delta are annually inundated up to 30 days (Figure 3a). The map of standard deviation of the annual flood duration shows ranges from a few days over the areas affected by floods during a short time span to 15 days close to permanent water bodies (Figure 3b).

Maps of errors made on land water surface duration with associated standard deviation are shown in Figure 3c and 3d over 2000-2015. Mixed pixels have been used to calculate the error for each pixel on land water surface duration, corresponding to the class 3 "mixed" of Sakamoto et al., 2007 classification. Standard deviation of error

is presented in Figure 3d. Maximal error and error standard deviation is obtained for pixels of potential flooding area in the delta. If short differences – lower than 20 ± 12 days – can be observed in the downstream part of the delta (over 69°N), longer differences (30 to 50 ± 15 to 20 days) are present in the upstream part. They can be attributed to the presence of small permanent lakes in this area. Important interannual differences can be observed between wetter (Figure 3e) and dryer (Figure 3f) years.

Surface water extent (the sum of permanent bodies and inundated areas) were also estimated applying the approach described in sub-section 3.1 for OLI images at 30 m of spatial resolution, and resampled at 500 m of spatial resolution. They were compared to MODIS-based surface water extent for the closest date (Table 1). Figure S3a, S3b and S3c present the maps of the surface water extent determined using MODIS, OLI 500 m and OLI 30 m respectively, acquired in July 2013. Medium and large scale (with a minimal size of 300 m) land water features are well detected as displayed on the zoomed part of images. Figure S3c present a zoom of surface water extent using OLI 30 m with permanent and inundated bodies. Surface water extent from OLI 500 m and MODIS are similar for both dates with differences lower than 20% (Table 1). For example in July 2013, land water surface is about 4,499 km² for OLI 500 and 3,798 km² for MODIS (Table 1). Percentages of common detection of surface water were estimated for the pixels detected as land water surface in the pair of satellite images. These percentages are 73 and 74 % for July 2013 and August 2013, respectively. Areas detected as water by both sensors corresponds to the main channels and connected floodplains. Differences appear on the boundaries of the commonly detected as inundated areas and at small-scales and can be attributed to the difference of acquisition dates between MODIS and OLI (Figure S4). These results highlight the robustness of the method of Sakamoto et al. (2007) for accurate land water surface retrievals. These surface water extent have been compared with surface water extent (channels and wetlands) determined by Emmerton et al. (2007) in Table 1. For MODIS, differences are lower than 15% and for OLI 500, differences are about 25% (Table 1).

However, the comparison between surface water extent estimated from OLI 30 m and MODIS 500 m shows important differences. In July 2013, surface water extent is about 3,798 km² from MODIS and 7,685 km² from OLI 30. The surface extents are higher for OLI 30 by a factor of 2 (Table 1). According to Emmerton et al., 2007, the Mackenzie Delta is composed of 49,000 lakes with a mean area of 0.0068 km² and 40% of the total number of lakes have an area inferior to 0.25 km². The pixel sizes of OLI 30 m and MODIS 500 m are approximately 0.0009 km² and 0.25 km², respectively. Thus, the high difference between the land water surfaces detected using OLI 30 m and MODIS is probably associated to a spatial sample bias. Small-scale water features detected from OLI cannot be detected from MODIS due to a lower spatial resolution.

Surface water extent determined using OLI 30 have been compared to Emmerton et al. (2007) surface water extent (including channels, wetlands and lakes). Emmerton et al., (2007) classified the Mackenzie Delta habitat in lakes, channels, wetlands and dry floodplains using information from a topographic maps derived from aerial photographies taken during the 1950's for low water periods. Differences between surface water extent of OLI 30 and Emmerton et al., (2007) are lower than 15 % (Table1).

In order to investigate the assumption of spatial sample bias associated with MODIS 500 m, a satellite validation of surface water extent is performed (Table 2). Permanent water and inundated surfaces have been calculated for MODIS, OLI 500 and OLI 30. For OLI 30 and OLI 500, pixels identified as surface water for the two dates are considered as permanent waters (Table 2). In July 2013, inundated surfaces are nearly equal, about 577 km² for

MODIS, 690 km² for OLI 500 and 627 km² for OLI 30 (Table 2). In August, inundated surfaces are equal to 250 km² and are 2.5 more important than OLI 30 (98 km²), if we consider OLI 30 as truth.

Time series of surface water extent in the Mackenzie Delta were derived from the 8-day maps of surface water extent (Figure 4). Surface extent water varies from 1,500 to 14,284 km² between 2000 and 2015 along the hydrological cycle. Each year, water surface extent is maximum in June in response to the spring ice break-up and snow melt that occurred in May (between day of year, DOY, 110 and 130 on average) in the Delta and decreases to reach a minimum in September, as previously observed by Goulding et al., 2009a, Goulding et al., 2009b. On average, during the study period, maximum surface water extent is ~9,600 km². The largest water surface extent was reached in June 2006 with an inundated area of 14,284 km², which represents ~85% of the delta total surface (Figure 4). Large surface water extents (~12,500 km²) were also detected in 2011 and 2013 in accordance with high discharge peaks reported these years (http://wateroffice.ec.gc.ca/) and the historic inundation that occurred in Aklavik in 2006 (Beltaos and Carter, 2009).

5.2 Alimetry-based water levels and their validation

The Mackenzie Delta is densely covered with altimetry tracks from the ERS-2, ENVISAT and SARAL missions that all were on the same nominal orbit. Twenty-two, twenty-seven and twenty-four altimetry virtual stations were built at the cross-section of an altimetry track with a water body for these three missions respectively (see Figure 5 for their locations). A water level temporal series is obtained for each virtual station.

The quality of altimetry-based water levels was evaluated using *in situ* gauge records. Only six virtual stations are located near *in situ* stations (with a distance lower than 20 km) for ERS-2 data, ten for ENVISAT and eight for SARAL data. Characteristics of these virtual stations are given in Table 3.

Altimetry-based water levels were validated using these virtual stations close enough (< 20 km) to *in situ* stations (6 comparisons for ERS-2, 10 for ENVISAT and 8 for SARAL). For ERS-2 and SARAL comparisons, the correlation r is low at the station 0114-c, i.e. -0.38 and 0.15 respectively (Table 3).

For ERS-2, quite high correlation coefficients are obtained for 4 virtual stations out of 6, with $r \geq 0.69$ and RMS ≤ 1 m (Table 3). For the two other stations, no correlation is observed (-0.38 and 0.08 for ERS-2-0114c and ERS-2-0200-d respectively with a RMS ≥ 1 m) (Table 3).

For ENVISAT, 8 out of 10 stations have a correlation coefficient ranging between 0.66 and 0.93 (Table 3). Except for ENV-0572-a, which is located 22 km away from the nearest in situ station, higher correlations were found when the river is larger at the VS (Table 3). For example, ENV-0114-b exhibits a negative correlation (r = -0.27) where the cross-section was only 150 m width (Table 3). This station is also located near the city of Inuvik. The presence of the town in the altimeter footprint could exert a strong impact on the radar echo and explain this low correlation.

For SARAL, 5 out of 6 virtual stations have a good correlation r coefficient higher than 0.76 with a low RMS (Table 3) due to its narrower footprint with an increase of the along-track sampling.

Comparisons between water levels derived from altimetry and *in-situ* are shown for two stations for ERS-2 (called ERS-2-0744-a and ERS-2-0439-a; Figure 6a and 7a), three for ENVISAT (ENV-0744-a, ENV-0439-a and ENV-0028-a; in Figure 6b, 7b and 8) and two for SARAL (SARAL-0744-a and SARAL-0439-a; Figure 6c and 7c).

Virtual station 0744-a is located in the downstream part of the delta, 0439-a in the center and 0028-a in the upstream part (Figure 5). For each station, water levels obtained by altimetry and water levels of *in situ* gauge are superposed (Figures 6, 7 and 8). Then, water level anomalies, which are computed as the average water level minus the water level, have been calculated for altimetry and in situ data.

The virtual station 0744-a is located in the North of the Mackenzie Delta (Figure 5). Water level time-series have been processed between 1995 and 2015 and compared to *in situ* data of the station 10MC010 for each mission ERS-2, ENVISAT and SARAL (Figure 6). *In situ* data are not continuous since river is frozen from October to April. With regard to altimetry, data have been acquired all the year but during frozen periods, water levels are unrealistic due to the presence of river ice. Thus, the processing is done only from the beginning of June to the end of September as for multispectral imagery treatment. The correlation r between altimetry water levels and in situ levels is 0.88 for ERS-2, 0.93 for ENVISAT and 0.99 for SARAL (Tables 3). For the three missions, RMS is weak, lower than 0.15 m (Tables 3). At this station, the variation of water level is about 2 m on average with an important water level in June that decreases to September (Figure 7a, 7c and 7e).

The virtual station ERS-2-0439-a is in the center of the Mackenzie Delta and water levels time-series have been done between 1995 and 2015 and compared to *in situ* data of the station 10MC008 for the three missions ERS-2, ENVISAT and SARAL (Figure 7). The correlation between altimetry water levels and water levels from in situ gauge is about 0.76 for ERS-2, 0.89 for ENVISAT and 0.96 for SARAL (Table 3). RMS is included between 0.35 and 0.5 m for the three missions. On average at this station, water levels variations are about 4 meters with a maximal water level in June that decreases to reach a minimal value in September (Figure 7a, 7c and 7e).

Water levels time-series between 2002 and 2010 at the virtual station ENV-0028-a located upstream of the Mackenzie Delta have been compared to *in situ* data of the station 10LC014 (Figure 8). A good correlation was found for this station too, with a coefficient correlation r of 0.83 and a RMS of 1.84 m (Table 3). For this station, variations of water levels are much higher with 9 m on average but reaching 12 m during the 2006 extreme event (Figure 8a). Water levels time-series were constructed only for ENVISAT mission since for the two others (ERS-2 and SARAL), altimetry water levels were not consistent exhibiting values around 70 meters. Therefore, water levels determined by altimetry and water level from *in situ* gauge have a difference, probably explained by the distance between virtual station and *in situ* gauge (16.31 km) since the slope is about -0.02m/km in the Delta (Hill et al., 2001). Moreover, the seasonal cyclic thawing and freezing of the active layer causes cyclic settlement and heave at decimeters levels, estimated to 20 cm (Szostak-Chrzanowski, 2013).

5.3 Time series of surface water storage anomalies in the Mackenzie Delta

The minimum water level of each inundated pixel was determined over the observation period. 8-day surface water levels maps were created after subtracting the minimum water level to water level at time t, using MODIS-based flood extent and altimetry-derived water levels in the entire delta from June to September. Example of water level maps are presented for 2006 at 4 different dates (in June, July, August and September), characterized as an historic flood (Figure 9).

Over the study period, water level maps show a realistic spatial pattern with a gradient of water level from south to north consistent with flow direction in the delta. On Figure 9a, in June 2006 for example, water levels are higher (about 5 m) upstream than downstream (about 0.5 m). The surface water storage reaches its maximal extent in

June (Figure 9a) and then decreases during the following months, reaching 1 m in September in the entire delta (Figure 9b, 9c and 9d).

The time series of surface water volume variations was estimated from 2000 to 2010 and then from 2013 to 2015, between June and September, following a similar approach as in Frappart et al., 2012 (Figure 10). Surface water storage was estimated from 2000 to 2003 using ERS-2 data, from 2003 to 2010 using ENVISAT data and from 2013 to 2015 using SARAL. Between 2010 and 2013, surface water storage could not be estimated due to lack of RA data over the delta. The impact of the presence of a virtual station located in the upstream part of the delta and the inclusion of ERS-2 data on our satellite-based surface water volume estimation were assessed. For ERS-2 and SARAL data, no virtual station was created in the upstream part due to unreliable water levels in the upstream part of the delta. During the SARAL observation period, *in situ* water levels from 10LC014 station were used. One curve corresponds to surface water volume with virtual station in the upstream part of the delta (2002-2015; red) and another one without virtual station in the upstream part of the delta (2000-2015; green). Correlations between river discharges and surface water volumes with and without (2002-2015) upstream virtual station are the same (0.66). Of the presence of a virtual station in the upstream part of the Mackenzie decreases the water volume by ~0.3 km^3 on average (Figure 10). The correlation is lower (0.63) when ERS-2 data are included in the analysis (2000-2015). The integration of ERS-2 data have a lower accuracy slight decrease the correlation between water storage and flux.

In term of temporal variability, a clear seasonal cycle is visible with a yearly maximum of water surface volume occurring in June (about 9.7 km^3 on average), followed by a decrease until September (Figure 10). The peak generally corresponds to the presence of the extensive flood covering the delta in June, and during summer, the volume decreases to reach its minimal in September (~0.2 km^3). The largest surface water volume happened in 2006 with a volume of 14.4 km^3 (Figure 10), known as an historic flood (Beltaos and Carter, 2009). These results showed that the satellite-based surface water volumes estimation are consistent with the Mackenzie River discharge, which is the main driver of the delta flooding.

6. Discussion

6.1 Spatio-temporal dynamics of surface water extent

Maps of surface water extent duration for annual average from 2000 to 2015 exhibit important spatio-temporal variations along the Mackenzie Delta (Figure 3a). Areas with open water present during the whole study period are located along the Mackenzie River and its tributaries. On the contrary, areas covered with open water for a duration lower than 30 days on the study period of 120 days are mostly located in the western upstream and eastern downstream parts of the delta but also in some locations in the western downstream part and along the Mackenzie mainstream (Figure 3a). They correspond to regions only inundated in June during the floods caused by spring ice break-up and snow melt occurring in May (see Figure 9 for the temporality of the flood extent). The central part of the Mackenzie is inundated between 40 and 70 days per year (Figure 3a). As it can be seen in Figure 9, this area is not continuously inundated but during two flood events in June in response to snowmelt and in August and September in response to an increase of river discharges of the Mackenzie River. This secondary peak ranges from 3,000 to 5,000 km^2 in comparison with the sooner one that ranges from 4,000 to 10,000 km^2 (Figure 4). Maps of difference between the duration of extreme surface water surface and the average duration water surface duration

from 2000 to 2015 were estimated for the large historic flood that occurred in 2006 (Figure 3e) and for the minimal flood that occurred in 2010 (Figure 3f). The whole Mackenzie Delta was practically covered of water in 2006, whereas large areas, especially in the downstream part of the delta, were not inundated in 2010 (Figure 3f).

6.2 Spatio-temporal dynamics of surface water levels in the Mackenzie delta

For all stations and RA missions, a strong seasonal cycle can be seen, with a maximum water level reach in June after the spring ice break-up and snow melt that decreases to reach a minimal value in September, in good accordance with the hydrological cycle of the Mackenzie Delta. The Delta is frozen from October to May and during spring-early summer, the freshwater meets an ice dam that was formed in winter, what provokes river discharges variations from 5,000 m^3 to 25,000 m^3 on average (http://wateroffice.ec.gc.ca/, Figure 1b). Then, these important variations provoke water levels increase and important floods each year in the delta. However, water levels variations as revealed from RA are not equal over the delta. In the upstream part, variations are 9 m on average, 4 m in the center and 3 m in the downstream part of the Mackenzie Delta.

Water level time-series from data acquired by the ENVISAT mission between June and September averaged over 2002-2010 are presented in Figure 11. Each time-series has been shifted manually and errors are not shown here for clarity purpose. Virtual stations used to discuss the spatio-temporal variations were chosen along the Mackenzie River from upstream to downstream and at similar latitudes on the Mackenzie River and its tributaries. They are represented using green dots for variations along the Mackenzie River and red triangles for latitudinal variations (Figure 11a). Time-series from Figure 11b are located along the Mackenzie River, number 1 is corresponding to the upstream part and number 8 to the downstream part. Logically, a stronger seasonal cycle is observed upstream than downstream. If the primary peak of flood that occurs in June clearly appears for all the stations, the secondary peak of August-September is not well marked for all the stations. This could be due to either local differences in the hydrodynamics of the river or due to the low temporal frequency of acquisition of the altimeters that is not sufficient to fully capture the whole specificities of the hydrological cycle (see Biancamaria et al., 2017 for instance). Latitudinal differences can also be noticed (Figure 11c). Larger annual amplitudes of water levels can be observed in the Mackenzie River than over its tributaries. The second flood event occurs earlier in the central part (August) than in the western and eastern parts (September).

6.3 Spatio-temporal dynamics of surface water storage

The spatio-temporal dynamics of surface water storage is presented in Figure 9 for 2006. A strong upstream-downstream gradient of water levels can be observed in June with water levels ranging 0 to 5 m from north to south (Figure 9a). It strongly decreases in July (0 to 1.5 m in Figure 9b) and does not appear in August (Figure 9c) and September (Figure 9d). For these two later months differences in water levels are more homogeneous of the whole delta (except in a region located around 135°W and between 68°N and 68°30'N in August°). Our results were compared to the ones estimated by Emmerton et al. (2007) under the assumption of a storage change as a rectangular water layer added to the average low-water volume for a stage variation from 1.231 m above sea level during low water period and 5.636 m above sea level at peak flood. Using this approach, Emmerton et al. (2007) found an increase in water volume of 14.14 km^3 over the floodplains and 7.68 km^3 over the channels. With our method, maximal water volume is around 9.6 km^3 in average and can reach 14 km^3. As it can be seen in Figure11, water levels present a strong decreasing gradient of amplitude over the delta towards the mouth and are, in average,

lower than 5.636 m from Emmerton et al. (2007). The difference of approaches is likely to account for such discrepancy. The comparison between storage and flux (discharge) exhibits a quite good correlation (R=0.66 with no time-lag) between these two quantities. Several studies demonstrated that there is no linear relationship between surface water extent, surface water volume and river discharge due to the presence of floodplains non-connected to the river (e.g., Frappart et al., 2005; Heimhuber et al., 2017). Due to the small area of the non-connected lakes present in the Mackenzie delta, they are detected in our approach based on the use of MODIS images at 500 m of spatial resolution, as mixture areas (except during the June flood event where almost all the delta is inundated and all the flooded areas are connected to the river). Only the floodplains connected to river are considered in this study.

7. Conclusion

This study provides surface water estimates (permanent water of rivers, lakes and inundated surfaces connected to the rivers) dynamics both in extent and storage in the Mackenzie Delta from 2000 to 2015 using MODIS images at 500 m of spatial resolution and altimetry-based water levels. Surface water exhibits a maximal extent in the beginning of June and decreases to reach a minimal value in September. In June, the extent of land water surface is on average about 9,600 km². The highest value was observed in 2006 (~14,284 km²), during the historic flood described by (Beltaos and Carter, 2009). Despite the lower resolution of MODIS images in comparison with Landsat-8 ones, surface water extent estimates are quite similar using both sensors over the river channels and the floodplains with an underestimation of 20% is found for MODIS. But, the numerous small lakes present in the Mackenzie Delta are not detected using MODIS. Nevertheless, the MODIS-based inundation product provides important information on flooding patterns along the hydrological cycle (flood events of June and August-September).

Virtual stations, or river/lake cross-section have been created across the Mackenzie Delta for the three radar altimetry missions (ERS-2, 1993-2003; ENVISAT, 2002-2010; SARAL, since 2013). Due to the lack of valid data acquired in interferometry SAR mode by Cryosat-2, no information on surface water levels is available in 2011 and 2012. The water levels determined by altimetry at those stations have been validated with *in situ* river levels with good correlation coefficient (> 0.8) for the three missions. The dense network of altimetry virtual stations composed of 22 stations for ERS-2, 27 for ENVISAT and 24 for SARAL allowed the analysis of the spatio-temporal variations of water levels across the delta.

The combination between land water extent determined by MODIS imagery and the water levels derived from altimetry permitted to estimate surface water storage variations in the Mackenzie Delta at 8-day temporal resolution. Maps of surface water levels showed a clear upstream-downstream gradient in June that decreases with time. Temporal variations in surface water volume calculated from 2000 to 2010 and from 2012 to 2015 showed a maximal volume in June (on average 9.6 km^3) and a minimal volume in September (about 0.1 km^3). A relatively strong correlation was found between surface water volume and the Mackenzie River discharges (R=0.66).

These products provide a unique long-term dataset that allows a continuous monitoring of the changes affecting the surface water reservoir before the launch of the NASA-CNES Surface Water and Ocean Topography (SWOT) mission in 2021. This approach can be applied to any other deltaic and estuarine environments as MODIS and altimetry data are available globally. The major limitations are i) the presence of clouds and dense vegetation cover

that prevent the use of MODIS images, ii) the relatively coarse spatial resolution of MODIS images, iii) the coarse coverage of altimetry tracks. They can be overcome i) using SAR images for flood extent monitoring as Frappart et al. (2005), ii) using images with a higher spatial resolution, iii) combing information the different altimetry missions orbiting simultaneously. The recent launches of Sentinel-1, Sentinel-2 and 3 offer new opportunities for flood extent monitoring at higher spatial (from 10 m to 300 m) and temporal (a few days) resolutions. Associated with Aquatic color radiometry (Mouw et al., 2015), the approach developed here should provide useful information for the study of fluvial particle transport along the river-to-coastal ocean continuum and its potential impacts on ecosystems.

7. Acknowledgments

This study was supported by an internship grant from LabEX Côte (Université de Bordeaux) and a PhD grant from Ministère de l'Enseignement Supérieur et de la Recherche and also by the CNES TOSCA CTOH grant. The authors also thank David Doxaran for fruitful discussion.

References

Alsdorf, D. E., Rodríguez, E. and Lettenmaier, D. P.: Measuring surface water from space, Rev. Geophys., 45(2), RG2002, doi:10.1029/2006RG000197, 2007.

Baup, F., Frappart, F. and Maubant, J.: Combining high-resolution satellite images and altimetry to estimate the volume of small lakes. Hydrol. Earth Syst. Sci., 18, 2007-2020, doi:10.5194/hess-18-2007-2014, 2014.

Beltaos, S. and Carter, T.: Field studies of ice breakup and jamming in the Mackenzie Delta, St John's, Newfoundland and Labrador., 2009.

Beltaos, S., Carter, T. and Rowsell, R.: Measurements and analysis of ice breakup and jamming characteristics in the Mackenzie Delta, Canada, Cold Reg. Sci. Technol., 82, 110–123, doi:10.1016/j.coldregions.2012.05.013, 2012.

Biancamaria, S., Frappart, F., Leleu, A.-S., Marieu, V., Blumstein, D., Desjonquères, J-D., Boy, F., Sottolichio, A. and Valle-Levinson A.: Satellite radar altimetry elevations performance over a 200 m wide river: Evaluation over the Garonne River, Advances in Space Research, 59, 128-146, 2017.

Birkett C.M.: The contribution of TOPEX/POSEIDON to the global monitoring of climatically sensitive lakes. Journal of Geophysical Research, 100, 179-204, 1995.

Cazenave, A., Bonnefond, P., Dominh, K. and Schaeffer, P.: Caspian Sea level from Topex-Poseidon altimetry: Level now falling, Geophys. Res. Lett., 24(8), 881–884, doi:10.1029/97GL00809, 1997.

Crétaux, J.-F., Jelinski, W., Calmant, S., Kouraev, A., Vuglinski, V., Bergé-Nguyen, M., Gennero, M.-C., Nino, F., Abarca Del Rio, R., Cazenave, A. and Maisongrande, P.: SOLS: A lake database to monitor in the Near Real Time water level and storage variations from remote sensing data, Adv. Space Res., 47(9), 1497–1507, doi:10.1016/j.asr.2011.01.004, 2011.

Crétaux, J.-F., Bergé-Nguyen, M., Leblanc, M. and Abarca Del Rio, R.: FLOOD MAPPING INFERRED FROM REMOTE SENSING DATA. n.d.

Crétaux J.F., Nielsen K., Frappart F., Papa F., Calmant S., Benveniste J. Submitted. Hydrological applications of satellite altimetry: rivers, lakes, man-made reservoirs, inundated areas. Satellite Altimetry Over Oceans and Land Surfaces, Detlef Stammer, Anny Cazenave (Eds), 2017

Emmerton, C. A., Lesack, L. F. W. and Marsh, P.: Lake Abundance, potential water storage, and habitat distribution in the Mackenzie River Delta, western Canadian Arctic: MACKENZIE DELTA WATER STORAGE, Water Resour. Res., 43(5), n/a-n/a, doi:10.1029/2006WR005139, 2007.

Emmerton, C. A., Lesack, L. F. W. and Vincent, W. F.: Nutrient and organic matter patterns across the Mackenzie River, estuary and shelf during the seasonal recession of sea-ice, J. Mar. Syst., 74(3–4), 741–755, doi:10.1016/j.jmarsys.2007.10.001, 2008.

Frappart, F., Seyler, F., Martinez, J.M., Léon, J.G., Cazenave, A.: Floodplain water storage in the Negro River basin estimated from microwave remote sensing of inundation area and water levels, Remote Sens. Environ., 99, 387-399, doi:10.1016/j.rse.2005.08.016, 2005.

Frappart, F., Calmant, S., Cauhope, M., Seyler, F. and Cazenave, A.: Preliminary results of ENVISAT RA-2-derived water levels validation over the Amazon basin, Remote Sens. Environ., 100(2), 252–264, doi:10.1016/j.rse.2005.10.027, 2006a.

Frappart, F., Minh, K. D., L'Hermitte, J., Cazenave, A., Ramillien, G., Le Toan, T. and Mognard-Campbell, N.: Water volume change in the lower Mekong from satellite altimetry and imagery data, Geophys. J. Int., 167(2), 570–584, doi:10.1111/j.1365-246X.2006.03184.x, 2006b.

Frappart, F., Papa, F., Güntner, A., Werth, S., Ramillien, G., Prigent, C., Rossow, W. B. and Bonnet, M.-P.: Interannual variations of the terrestrial water storage in the Lower Ob' Basin from a multisatellite approach, Hydrol. Earth Syst. Sci., 14(12), 2443–2453, doi:10.5194/hess-14-2443-2010, 2010.

Frappart, F., Papa, F., Santos da Silva, J., Ramillien, G., Prigent, C., Seyler, F. and Calmant, S.: Surface freshwater storage and dynamics in the Amazon basin during the 2005 exceptional drought, Environ. Res. Lett., 7(4), 044010, doi:10.1088/1748-9326/7/4/044010, 2012.

Frappart, F., Papa, F., Malbeteau, Y., León, J., Ramillien, G., Prigent, C., Seoane, L., Seyler, F. and Calmant, S.: Surface Freshwater Storage Variations in the Orinoco Floodplains Using Multi-Satellite Observations, Remote Sens., 7(1), 89–110, doi:10.3390/rs70100089, 2015a.

Frappart, F., Papa, F., Marieu, V., Malbeteau, Y., Jordy, F., Calmant, S., Durand, F. and Bala, S.: Preliminary Assessment of SARAL/AltiKa Observations over the Ganges-Brahmaputra and Irrawaddy Rivers, Mar. Geod., 38(sup1), 568–580, doi:10.1080/01490419.2014.990591, 2015b.

Frappart, F., Legrésy, B., Niño, F., Blarel, F., Fuller, N., Fleury, S., Birol, F. and Calmant, S.: An ERS-2 altimetry reprocessing compatible with ENVISAT for long-term land and ice sheets studies, Remote Sens. Environ., 184, 558–581, doi:10.1016/j.rse.2016.07.037, 2016.

Fu, L.-L. and Cazenave, A., Eds.: Satellite altimetry and earth sciences: a handbook of techniques and applications, Academic Press, San Diego., 2001.

Goulding, H. L., Prowse, T. D. and Bonsal, B.: Hydroclimatic controls on the occurrence of break-up and ice-jam flooding in the Mackenzie Delta, NWT, Canada, J. Hydrol., 379(3–4), 251–267, doi:10.1016/j.jhydrol.2009.10.006, 2009a.

Goulding, H. L., Prowse, T. D. and Beltaos, S.: Spatial and temporal patterns of break-up and ice-jam flooding in the Mackenzie Delta, NWT, Hydrol. Process., 23(18), 2654–2670, doi:10.1002/hyp.7251, 2009b.

Heimhuber, V., Tulbure, M.G. and Broich, M.: Modeling multidecadal surface water inundation dynamics and key drivers on large river basin scale using multiple time series of Earth-observation and river flow data, Water Resources Research, 53, 1251-1269, doi:10.1002/2016WR019858, 2017.

Hill, P. R., Lewis, C. P., Desmarais, S., Kauppaymuthoo, V. and Rais, H.: The Mackenzie Delta: sedimentary processes and facies of a high-latitude, fine-grained delta, Sedimentology, 48(5), 1047–1078, doi:10.1046/j.1365-3091.2001.00408.x, 2001.

Holmes, R. M., McClelland, J. W., Peterson, B. J., Tank, S. E., Bulygina, E., Eglinton, T. I., Gordeev, V. V., Gurtovaya, T. Y., Raymond, P. A., Repeta, D. J., Staples, R., Striegl, R. G., Zhulidov, A. V. and Zimov, S. A.:

Seasonal and Annual Fluxes of Nutrients and Organic Matter from Large Rivers to the Arctic Ocean and Surrounding Seas, Estuaries Coasts, 35(2), 369–382, doi:10.1007/s12237-011-9386-6, 2012.

Huete A.R., Liu H.Q., Batchily K. and van Leeuwen W.: A comparison of vegetation indices over a global set of TM images for EOS-MODIS. Remote Sens. Environ. 59, 440-451, 1997.

Klein, I., Gessner, U., Dietz, A.J., Kuenzer, C.: Global WaterPack - A 250 m resolution dataset revealing the daily dynamics of global inland water bodies. Remote Sens. Environ., 198, 345-362, doi.org/10.1016/j.rse.2017.06.045, 2017.

Lesack, L. F. W. and Marsh, P.: River-to-lake connectivities, water renewal, and aquatic habitat diversity in the Mackenzie River Delta: RIVER-TO-LAKE WATER CONNECTIVITIES, Water Resour. Res., 46(12), n/a-n/a, doi:10.1029/2010WR009607, 2010.

Macdonald, R. W. and Yu, Y.: The Mackenzie Estuary of the Arctic Ocean, in Estuaries, vol. 5H, edited by P. J. Wangersky, pp. 91–120, Springer-Verlag, Berlin/Heidelberg. [online] Available from: http://link.springer.com/10.1007/698_5_027 (Accessed 14 December 2016), 2006.

Mouw, C. B., Greb, S., Aurin, D., DiGiacomo, P. M., Lee, Z., Twardowski, M., Binding, C., Hu, C., Ma, R., Moore, T., Moses, W. and Craig, S. E.: Aquatic color radiometry remote sensing of coastal and inland waters: Challenges and recommendations for future satellite missions, Remote Sens. Environ., 160, 15–30, doi:10.1016/j.rse.2015.02.001, 2015.

Muhammad, P., Duguay, C. and Kang, K.-K.: Monitoring ice break-up on the Mackenzie River using MODIS data, The Cryosphere, 10(2), 569–584, doi:10.5194/tc-10-569-2016, 2016.

Ogilvie, A., Belaud, G., Delenne, C., Bailly, J.-S., Bader, J.-C., Oleksiak, A., Ferry, L. and Martin, D.: Decadal monitoring of the Niger Inner Delta flood dynamics using MODIS optical data, J. Hydrol., 523, 368–383, doi:10.1016/j.jhydrol.2015.01.036, 2015.

Papa, F., Prigent, C., Aires, F., Jimenez, C., Rossow, W.B. and Matthews E.: Interannual variability of surface water extent at the global scale, 1993-2004., Journal of geophysical research, 115, D12111, doi: 10.1029/2009JD012674, 2010.

Pekel, J., Cottam, A., Gorelick, N., and Belward, A.S.: High resolution mapping of global surface water and its long-term changes, Nature, 540, 418–422, doi: 10.1038/nature20584, 2016

Peterson, B. J., Holmes, R. M., McClelland, J. W., Vörösmarty, C. J., Lammers, R. B., Shiklomanov, A. I., Shiklomanov, I. A. and Rahmstorf, S.: Increasing River Discharge to the Arctic Ocean, Science, 298(5601), 2171–2173, doi:10.1126/science.1077445, 2002.

Rees W.G.: Physical principles of remote sensing, Cambridge University press, 460 p, 2013.

Sakamoto, T., Van Nguyen, N., Kotera, A., Ohno, H., Ishitsuka, N. and Yokozawa, M.: Detecting temporal changes in the extent of annual flooding within the Cambodia and the Vietnamese Mekong Delta from MODIS time-series imagery, Remote Sens. Environ., 109(3), 295–313, doi:10.1016/j.rse.2007.01.011, 2007.

Santos da Silva, J., Calmant, S., Seyler, F., Rotunno Filho, O. C., Cochonneau, G. and Mansur, W. J.: Water levels in the Amazon basin derived from the ERS 2 and ENVISAT radar altimetry missions, Remote Sens. Environ., 114(10), 2160–2181, doi:10.1016/j.rse.2010.04.020, 2010.

Smith, L. C.: Satellite remote sensing of river inundation area, stage, and discharge: a review, Hydrol. Process., 11(10), 1427–1439, doi:10.1002/(SICI)1099-1085(199708)11:10<1427::AID-HYP473>3.0.CO;2-S, 1997.

Squires, M. M., Lesack, L. F. W., Hecky, R. E., Guildford, S. J., Ramlal, P. and Higgins, S. N.: Primary Production and Carbon Dioxide Metabolic Balance of a Lake-Rich Arctic River Floodplain: Partitioning of Phytoplankton, Epipelon, Macrophyte, and Epiphyton Production Among Lakes on the Mackenzie Delta, Ecosystems, 12(5), 853–872, doi:10.1007/s10021-009-9263-3, 2009.

Stocker, T. F. and Raible, C. C.: Water cycles shifts gear, Nature, 434, 2005.

Szostak-Chrzanowski, A.: Study of Natural and Man-induced Ground Deformation in MacKenzie Delta Region, Acta Geodyn. Geomater., 1–7, doi:10.13168/AGG.2013.0060, 2013.

Tulbure, M.G., Broich, M., Stehman, S.V., Kommareddy A.: Surface water extent dynamics from the three decades of seasonally continuous Landsat time series at subcontinental scale in a semi-arid region. Remote Sens. Environ., 178, 142-157, doi.org/10.1016/j.rse.2016.02.034, 2016.

Ulaby, F. T., Moore, R. K. and Fung, A. K.: Microwave remote sensing: Active and passive. Volume 1 - Microwave remote sensing fundamentals and radiometry. [online] Available from: https://ntrs.nasa.gov/search.jsp?R=19820039342 (Accessed 15 December 2016), 1981.

U.S. Geological Survey. Product guide, Landsat surface reflectance-derived spectral indices. Version 3.3. December 2016.

Verpoorter, C., Kutser, T., Seekell, D. A. and Tranvik, L. J.: A global inventory of lakes based on high-resolution satellite imagery, Geophys. Res. Lett., 41(18), 6396–6402, doi:10.1002/2014GL060641, 2014.

Verron, J., Sengenes, P., Lambin, J., Noubel, J., Steunou, N., Guillot, A., Picot, N., Coutin-Faye, S., Sharma, R., Gairola, R. M., Murthy, D. V. A. R., Richman, J. G., Griffin, D., Pascual, A., Rémy, F. and Gupta, P. K.: The SARAL/AltiKa Altimetry Satellite Mission, Mar. Geod., 38(sup1), 2–21, doi:10.1080/01490419.2014.1000471, 2015.

Wang, M. and Shi, W. Estimation of ocean contribution at the MODIS near-infrared wavelengths along the east coast of the U.S.: Two case studies. Geophys. Res. Lett., 32, L13606, 2005.

Xiao, X., Boles, S., Liu, J., Zhuang, D., Frolking, S., Li, C., Salas, W., Moore, B. Mapping paddy rice agriculture in southern China using multi-temporal MODIS images. Remote Sens. Environ. 95, 480–492. doi:10.1016/j.rse.2004.12.009, 2005

Zelli C.: ENVISAT RA-2 Advances Radar Altimeter: instrument design and pre-launch performance assessment review. Acta Astronautica. 44, 323-33, 1999.

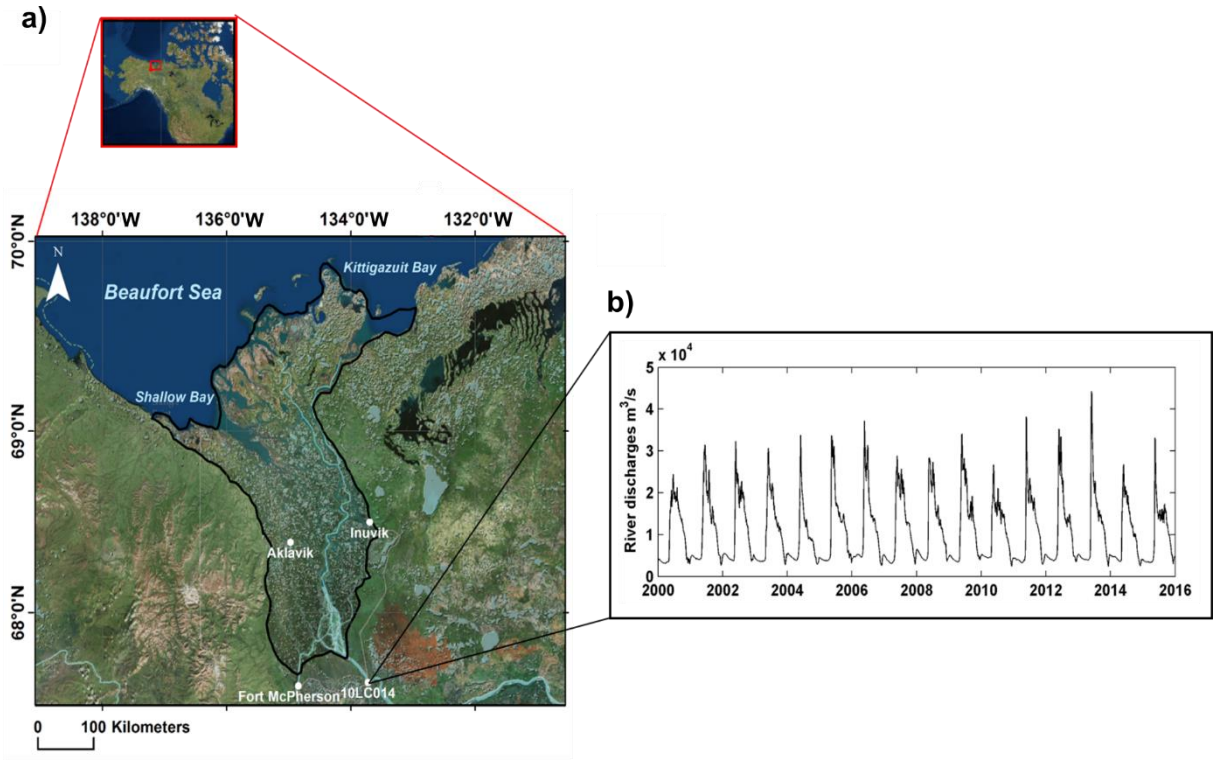

Figure 1: (a) Location of the Mackenzie Delta at the mouth of the Mackenzie River in the Northwest Territories of Canada (b) river discharges of the Mackenzie River at 10LC014 station from 2000 to 2015 (133°W, 67°N), 30 km upstream the Mackenzie Delta.

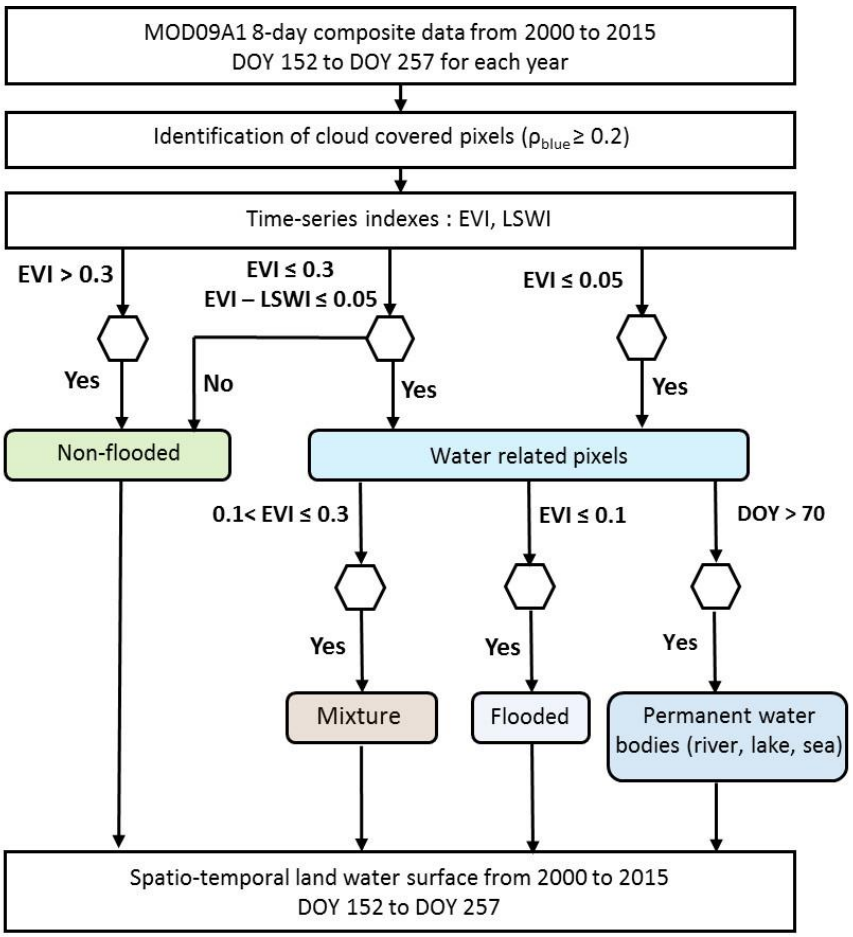

Figure 2: Flow-chart of the method (adapted from Sakamoto et al., 2007) used to classify each pixel of the multispectral images acquired over the Mackenzie Delta in 4 categories (non-flooded, mixed, flooded and permanent water bodies) for each year from 2000 to 2015 using MODIS 8-day composite data from the day of the year (DOY) 169 to 257.

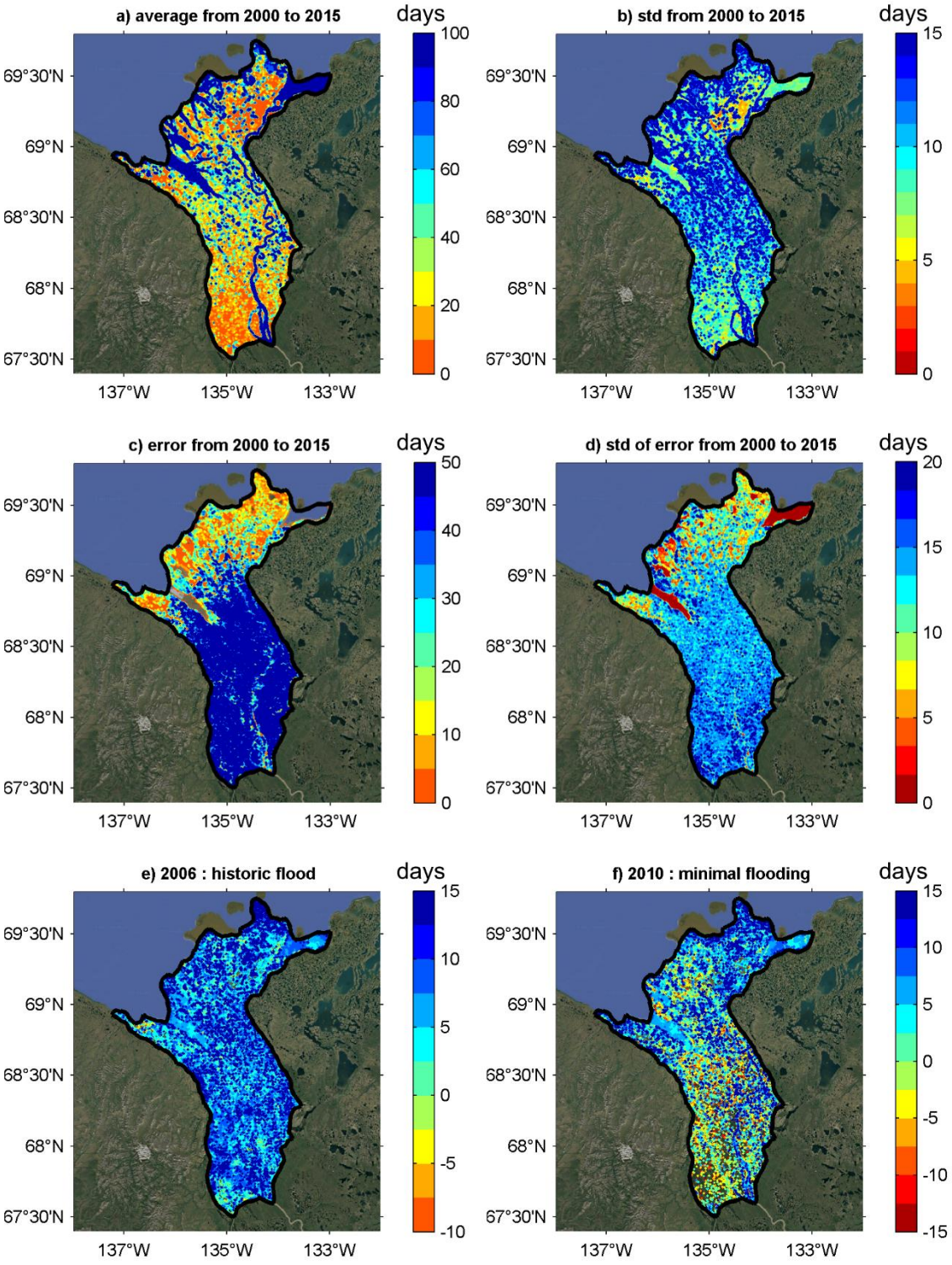

Figure 3: Maps of surface water extent duration for (a) annual average from 2000 to 2015, (b) annual standard deviation from 2000 to 2015, (c) error average from 2000 to 2015, (d) standard deviation of error from 2000 to 2015, difference between annual average land water surface duration from 2000 to 2015 and land water surface duration during (e) 2006 associated with the highest flood event, and (f) 2010 associated with the lowest flood event recorded over the period.

5

Table 1: Validation of surface water extents (km²) determined using OLI 30 m, OLI 500 m, and MODIS 500 m images with Emmerton et al. (2007)

	MODIS : 04/07/2013 **OLI : 01/07/2013**	**MODIS : 05/08/2013** **OLI : 02/08/2013**
MODIS 500 m	3,798	3,298
OLI 500 m	4,499	3,859
Emmerton et al., 2007 (channels+wetlands, km²)	3,358	3,358
Difference between MODIS 500 and Emmerton et al., 2007	440 km² (13 %)	60 km² (2 %)
Difference between OLI 500 and Emmerton et al., 2007	1,141 (34 %)	500 (15 %)
OLI 30 m	7,685	7,156
Emmerton et al., 2007 (channels+lakes+wetlands, km²)	6,689	6,689
Difference between OLI 30 and Emmerton et al., 2007	996 km² (13 %)	467 km² (7 %)

Table 2: Satellite validation of surface water extent using OLI 30, OLI 500 and MODIS 500 m.

Date	Permanent water MODIS (km^2)	Permanent water OLI 500 (km^2)	Permanent water OLI 30 (km^2)	Inundated surfaces MODIS (km^2)	Inundated surfaces OLI 500 (km^2)	Inundated surfaces OLI 30 (km^2)
MODIS : 04/07/2013 OLI : 01/07/2013	3,167	3,809	7,058	577	690	627
MODIS : 05/08/2013 OLI : 02/08/2013	2,885	3,809	7,058	250	50	98

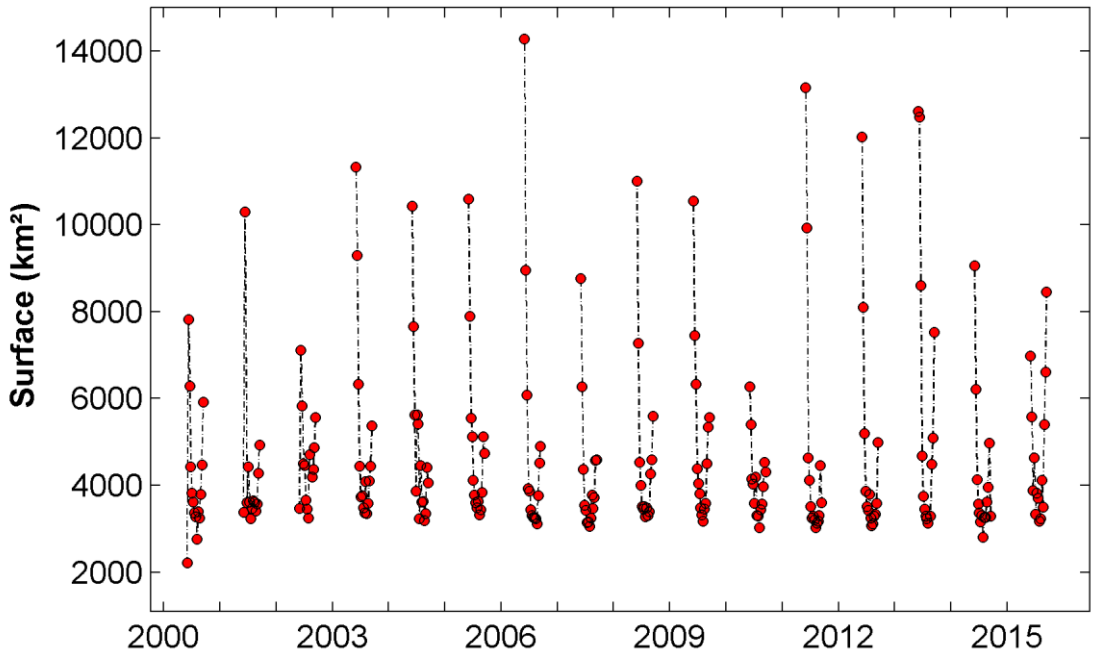

Figure 4: Time series of surface water extent from 2000 to 2015, between June and September, derived from the MODIS images.

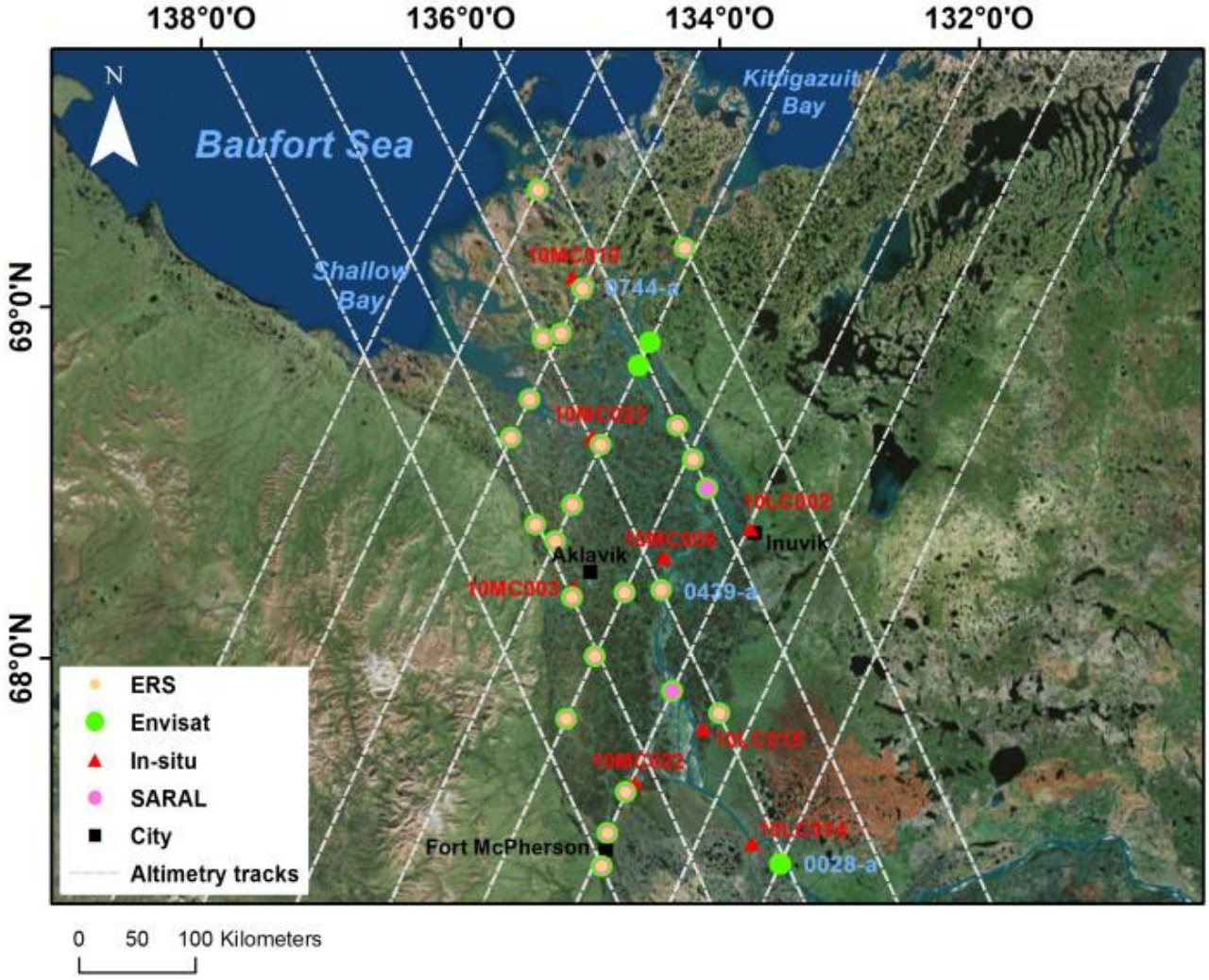

Figure 5: Locations of virtual stations (VS) in the Mackenzie Delta for ERS-2 (yellow dots), Envisat (green dots) and SARAL (purple dots) altimetry missions. Altimetry tracks appear in grey. *In situ* stations are represented using red triangles

Table 3: Statistic parameters obtained between altimetry-based water levels from altimetry multi-mission and *in situ* water levels

Virtual station (SV)	In situ station	Altimetry mission	Distance (km)	River width at VS (m)	N	r	RMS (m)	R^2	Bias (m)	Bias ICESat (m)
		ERS-2			5	0.76	0.5	0.58	0.55	1.36
0439-a	10MC008	ENVISAT	11.44	1950	24	0.89	0.5	0.81	0.15	0.65
		SARAL			8	0.96	0.35	0.93	-0.95	-0.15
		ERS-2			20	0.69	0.7	0.47	-	-
0983-c	10MC003	ENVISAT	3.1	360	26	0.66	0.89	0.44	-	-
		SARAL			6	0.9	0.4	0.8	-	-
		ERS-2			14	-0.38	2.82	0.14	-	-
0114-c	10MC022	ENVISAT	1.9	430	23	0.8	1.17	0.64	-	-
		SARAL			7	0.14	0.73	0.02	-	-
		ERS-2			17	0.08	4.3	0	-	-
0200-d	10MC023	ENVISAT	4.11	630	22	0.87	0.33	0.75	-	-
		SARAL			6	0.76	0.3	0.57	-	-
		ERS-2			5	0.88	0.1	0.77	-	-1.28
0744-a	10MC010	ENVISAT	5.16	850	24	0.93	0.15	0.87	-	-1.17
		SARAL			2	0.99	0.15	0.99	-	-2.19
		ERS-2			20	0.92	0.83	0.86	-	-
0439-d	10LC015	ENVISAT	7.2	380	28	0.65	1.75	0.43	-	-
		SARAL			5	0.95	1.3	0.9	-	-
0525-a	10MC002	ENV	16.31	500	29	0.77	1.45	0.6	-	-
0028-a	10LC014	ENV	16.05	1360	17	0.83	1.84	0.7	-	2.35

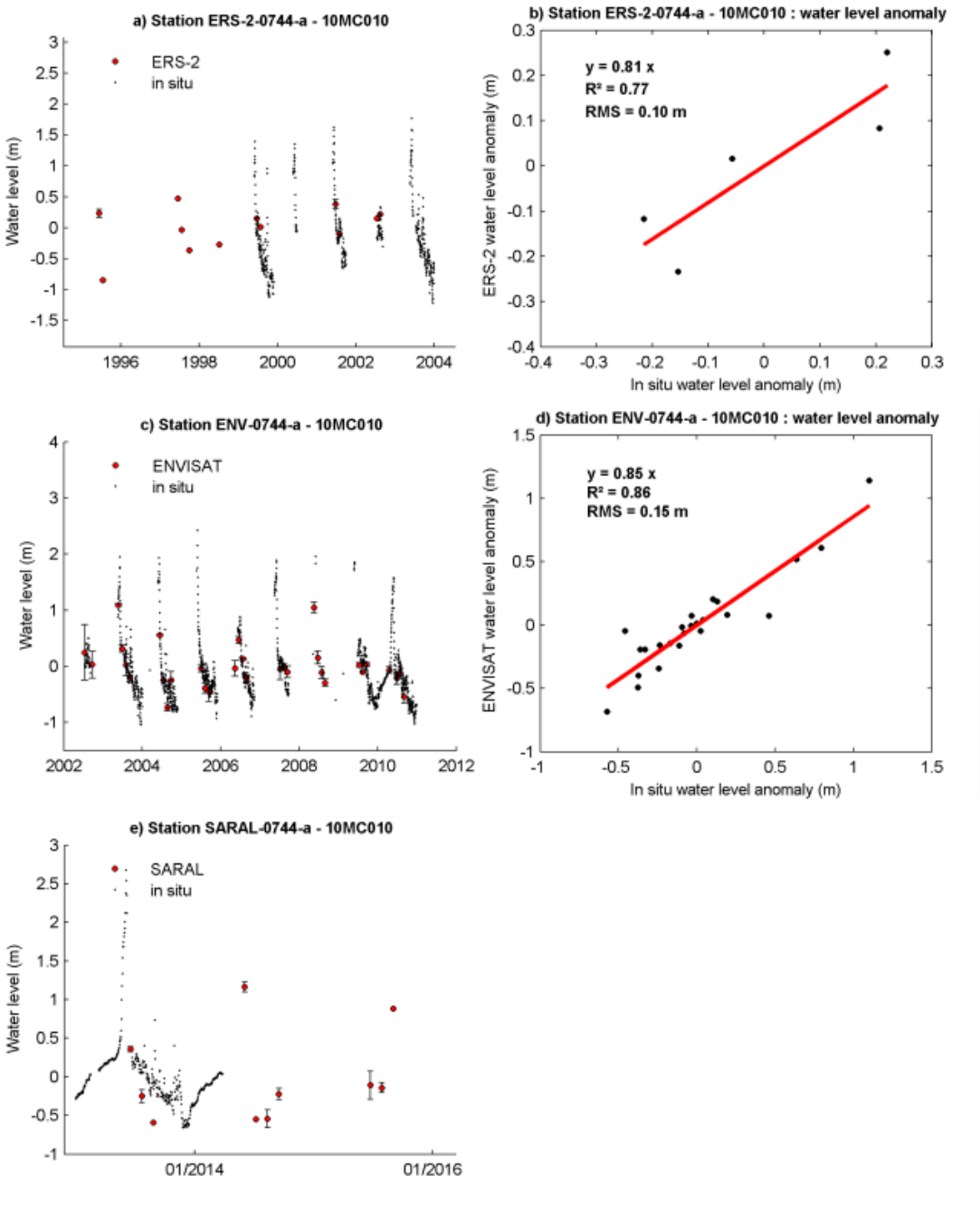

Figure 6: Altimetry-based water levels from 1995 to 2015 compared with in situ water levels for the station 0744-a located in the downstream part in the Mackenzie Delta (a) using ERS-2 mission and (b) water level anomaly with statistic parameters, (c) using ENVISAT mission and (d) water level anomaly with statistic parameters and (e) using SARAL mission

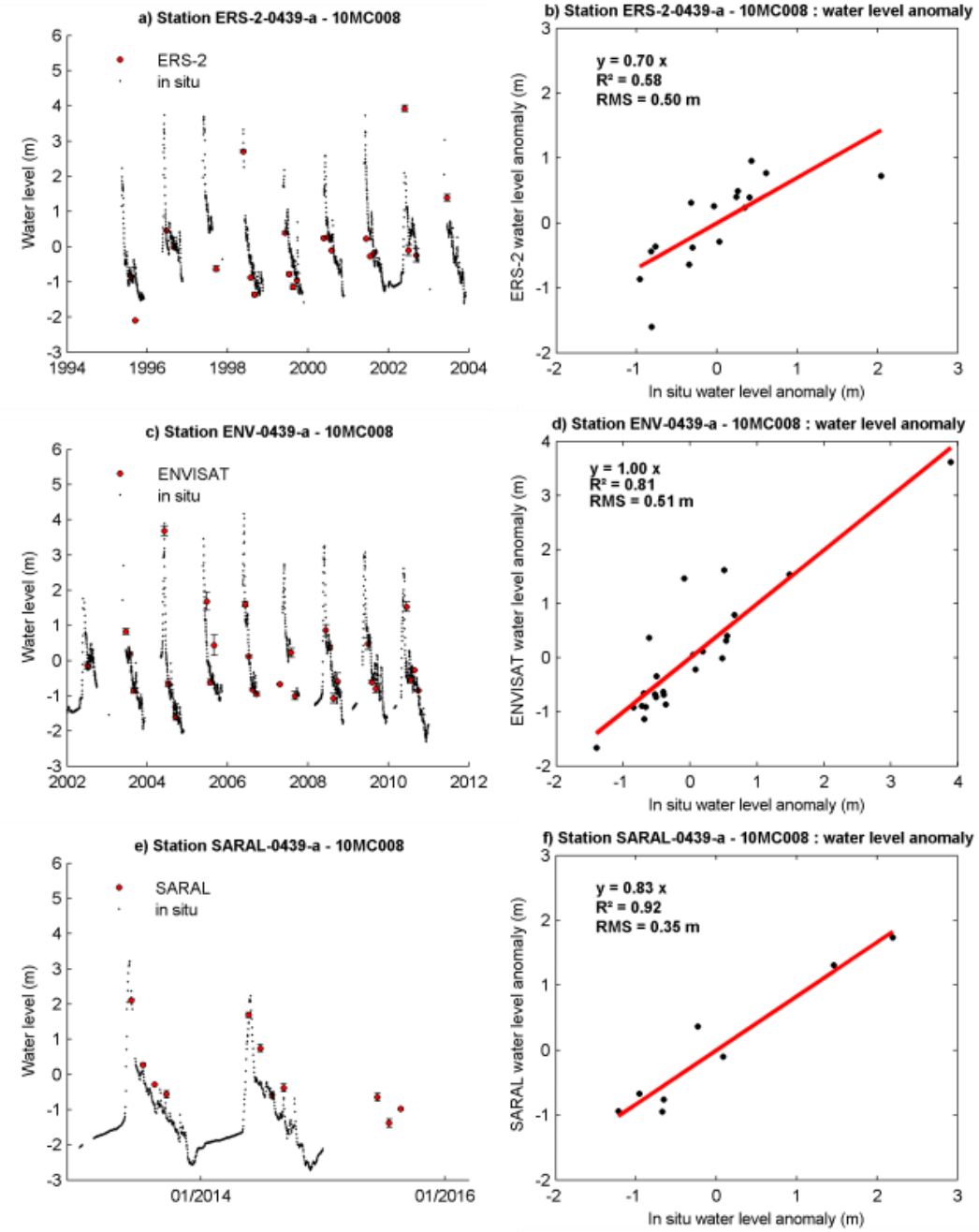

Figure 7: Altimetry-based water levels from 1995 to 2015 compared with in situ water levels for the station 0439-a located in the centre in the Mackenzie Delta (a) using ERS-2 mission and (b) water level anomaly with statistic parameters, (c) using ENVISAT mission and (d) water level anomaly with statistic parameters, (e) using SARAL mission and (f) water level anomaly with statistic parameters.

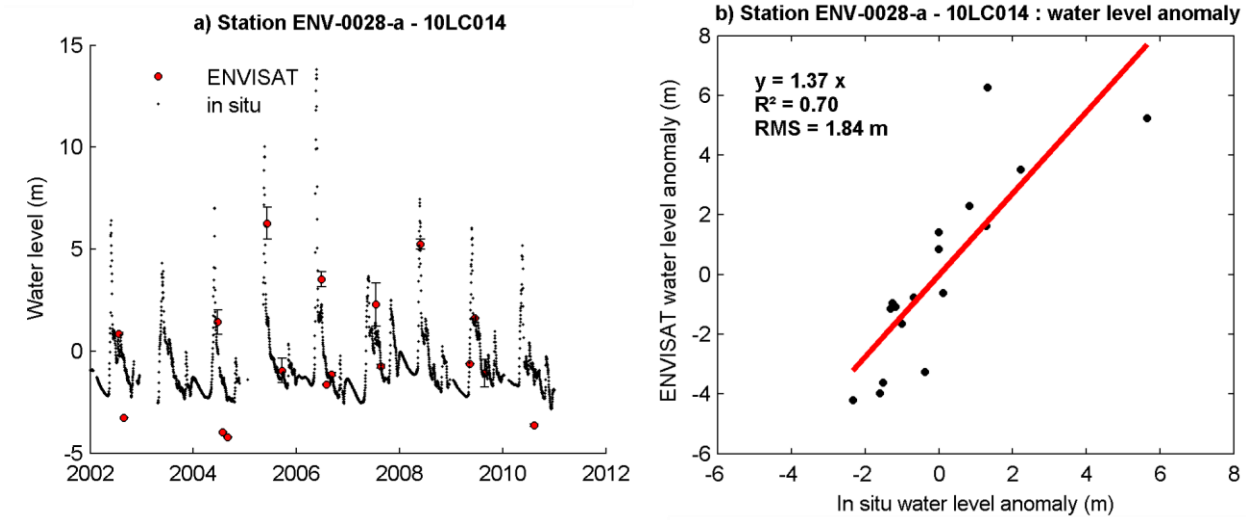

Figure 8: Altimetry-based water levels from 2002 to 2010 compared to in situ water levels for the station 0439-a located in the centre in the Mackenzie Delta (a) using ENVISAT mission and (b) water level anomaly with statistic parameter

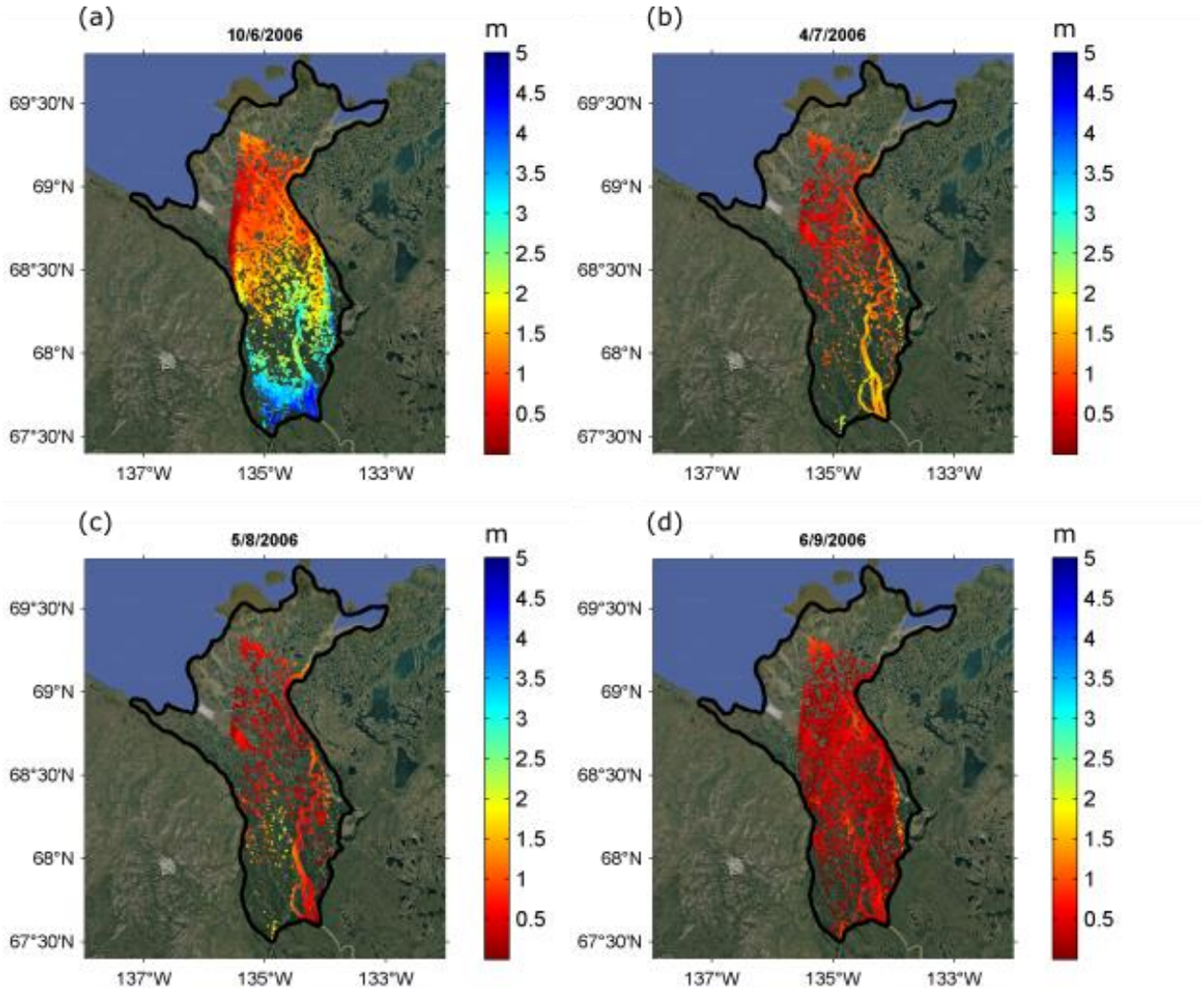

Figure 9: Water level maps in the Mackenzie Delta in 2006 (historic flood) obtained combining inundated surfaces determined using MODIS images with altimetry-derived water levels (a) in June, (b) in July, (c) in August and (d) in September

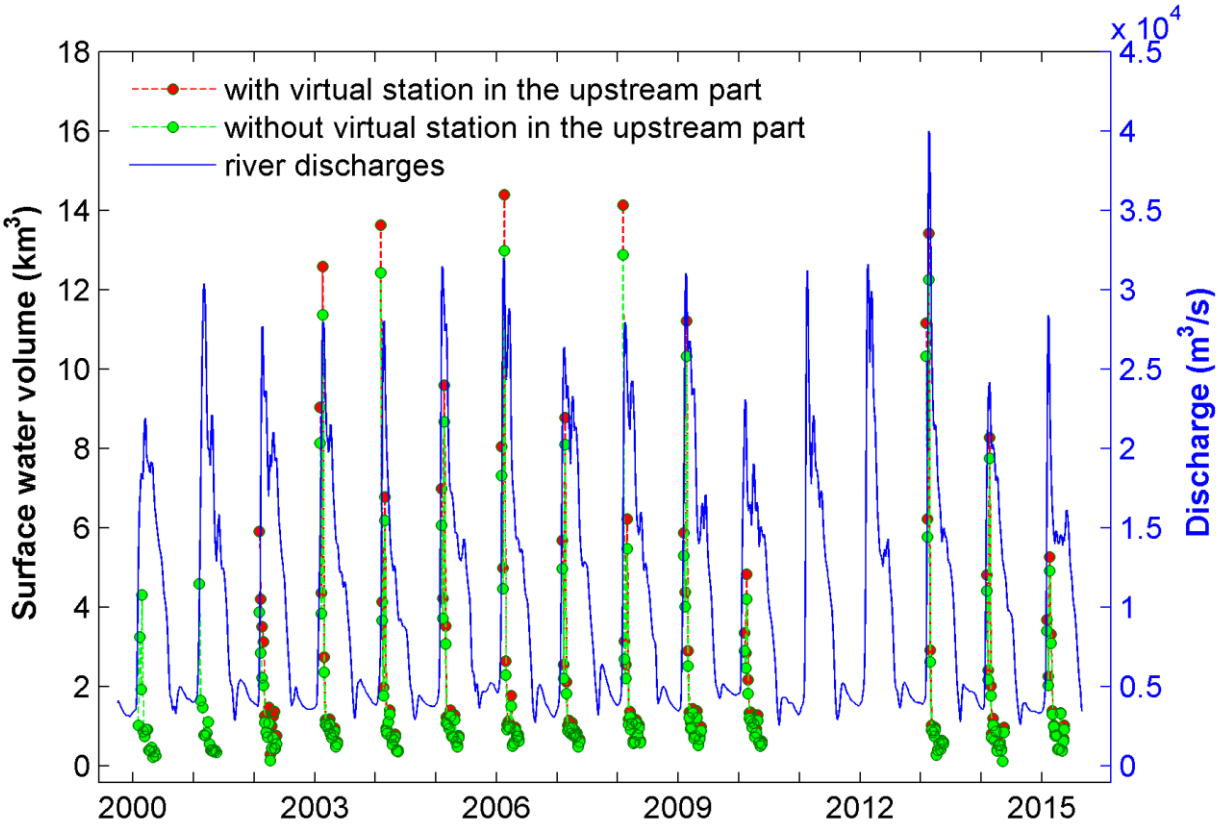

Figure 10: Surface water volume from 2000 to 2015, determined by combining inundated surfaces from MODIS with altimetry data. 167 red points correspond to surface water volume obtained with a virtual station located in the upstream part of the Delta, green points to surface water volume without a virtual station located in the upstream part of the Delta. The Mackenzie River Delta discharges at 10LC014 gauge station appear in blue.

5

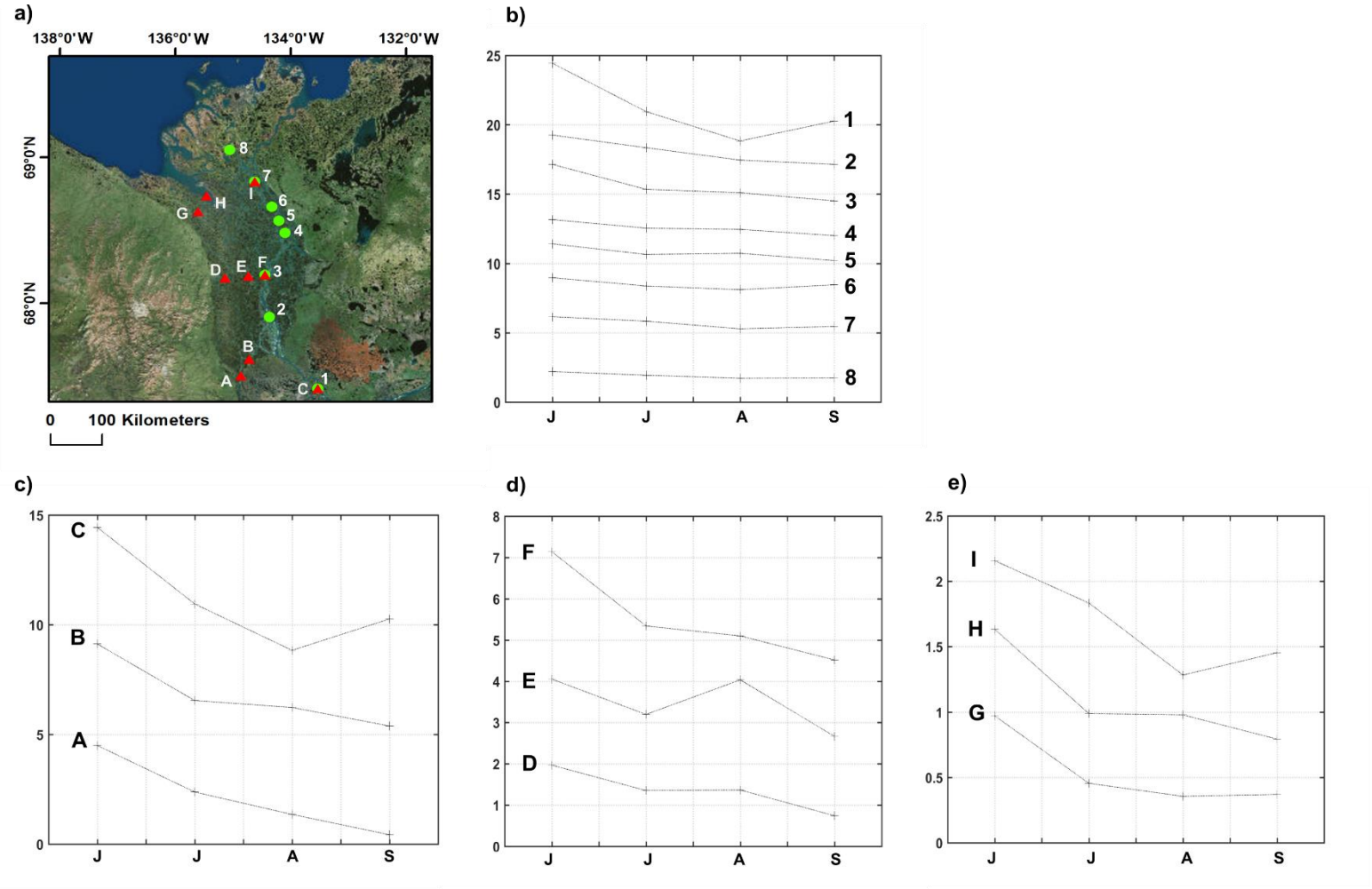

Figure 11: Temporal and spatial variations of surface water levels in the Mackenzie Delta a) Location of virtual stations used to analyse spatial variations, green dots are corresponding to latitudinal variations along the Mackenzie River (from number 1 to 8) and red triangles are corresponding to longitudinal variations at 3 different latitudes (letters from A to I), b) surface water levels time-series along the Mackenzie River at different latitudes, c), d) and e) show surface water levels time series at 3 different latitudes with 3 virtual stations at each latitude to analyse longitudinal spatial variations.